Nanoporous membranes

DOI: 10.1002/smll.200600398

Confined Diffusion in Ordered Nanoporous Alumina Membranes**

*J. Hohlbein, M. Steinhart, C. Schiene-Fischer, A. Benda, M. Hof, and Christian G. Hübner**

Appropriate anodizing of aluminum yields extended membranes containing aligned nanopores with pore diameters of a few tens of nanometers, high pore density, and well-defined porosity.[1,2] Such membranes may be used for separation as well as for analytical purposes.[3,4] These applications are associated with motions of molecules inside the pores. Detailed knowledge of the diffusive behavior of the molecules on the nanoscopic[5–7] scale is therefore crucial for the understanding and optimization of prospective device structures. Here we show that fluorescence correlation spectroscopy (FCS) is a versatile tool to quantitatively evaluate the mobility of fluorescent probe molecules and their interactions with the pore walls.[8] Autocorrelation analysis of the fluorescence signal reveals apparent one-dimensional (1D) diffusion of the probe molecules inside the pores with a dwell time in the confocal volume up to 19 times longer than in the case of bulk diffusion. Analyzing the fluorescence lifetime changes in the nanostructure we find that no collisional quenching of fluorescence occurs at the pore walls. One-dimensional FCS in ordered nanoporous alumina is potentially an efficient tool to study macromolecules in channel-type confinement and to evaluate the performance of membranes in separation and sensing. Our approach may also be applicable in the context of fluid transport in nanoscale pores.[9]

The ultimate limit in chemical analysis is the detection of individual molecules.[10] Exploiting laser-induced fluorescence in a confocal arrangement, single-molecule detection (SMD) in bulk solution has been applied to, for instance, the study of protein folding,[11–13] protein–protein interaction,[14] and DNA hybridization.[15] This technique, however, suffers from two limitations. First, in a typical single-molecule-solution experiment, the concentration of sample molecules is limited to 100 pM to keep the probability of double occupancy of the detection volume low. A reduction of the detection volume enables higher analyte concentrations. To this end, confinement of the laser field[16] or confinement of the solution-accessible volume fraction using a single microchannel has been studied.[17] Second, the transit time of the freely diffusing molecules through the confocal volume restricts the timescale of internal dynamics that can be explored by this method. The 1D diffusion along the long axis of the ellipsoidal confocal volume expected in a channel-type confinement would increase the residence time of the probe molecules in the focal volume and therefore extend the timeframe within which their internal dynamics can be probed. The high degree of order in the nanoporous membranes as compared to less ordered mesoporous materials[5–7] represents a system where all pores are oriented parallel, have uniform diameter, and extend from one side of the membrane to the other for up to tens of micrometers, which is advantageous in this context.

Using laser-induced fluorescence in a confocal microscope, we study the behavior of fluorescent probe molecules inside nanoporous alumina by means of FCS. As a model system we selected ordered porous alumina membranes prepared following the two-step procedure reported by Masuda and Fukuda.[1,18] The membranes feature a pore diameter of 35–40 nm, a porosity (volume fraction of the pores) of 20–25 %, and a thickness of 35 μm (see Supporting Information). The aspect ratio of the pores is thus ≈1000. We have implemented the nanopores-confinement technique in a state-of-the-art fluorescence correlation spectroscopy setup.[19] The alignment of the long axis of the pores with the optical axis of the confocal microscope (Figure 1a) forces the probe molecules to diffuse parallel to the long axis of the laser focus. We use the coverglass thickness-correction capability of the microscope objective to compensate for the mismatch of refractive indices between water ($n=1.33$) and the water-filled membrane treated as an effective medium with $n=1.57$,[20] which is possible due to the similarity of the refractive indices of glass ($n=1.518$) and the water-filled porous alumina (see Supporting Information).

Prior to the measurements, we soaked the membrane in a 107 μM bovine serum albumine (BSA) solution in order to prevent nonspecific adsorption of analytes. This treatment leads to an average BSA coverage of about 1 nm at the pH value of the solution we use.[21] Widely used fluorescent labels were selected as probe molecules, namely the autofluorescent enhanced green fluorescent protein (EGFP) and Alexa Fluor 488. EGFP is the F64L/S65T variant of the autofluorescent compact globular green fluorescent protein

[*] Prof. C. G. Hübner
University Halle, Physics Department
Hoher Weg 8, 06120 Halle (Germany)
Fax: (+49) 345-552-7221
E-mail: christian.huebner@physik.uni-halle.de
J. Hohlbein, Dr. M. Steinhart
Max Planck Institute of Microstructure Physics
Weinberg 2, 06120 Halle (Germany)
Dr. C. Schiene-Fischer
Max Planck Research Group for Enzymology of Protein Folding
Weinbergweg 22, 06120 Halle (Germany)
Dr. A. Benda, Dr. M. Hof
J. Heyrovsky Institute of Physical Chemistry
Academy of Sciences of the Czech Republic
Dolejkova 3, 18223 Prague 8 (Czech Republic)

[**] This work was supported by the Volkswagen Foundation (Thematic Impetus Interplay between Molecular Conformations and Biological Function, Az., I/80 778/779/780). J.H. acknowledges financial support from the German Academic Exchange Service (DAAD). A.B. and M.H. thank the Grant Agency of the Czech Republic (A.B. via 203/05/2308) and the Ministry of Education, Youth, and Sports of the Czech Republic (M.H. via LC06063) for financial support.

Supporting information for this article is available on the WWW under http://www.small-journal.com or from the author.

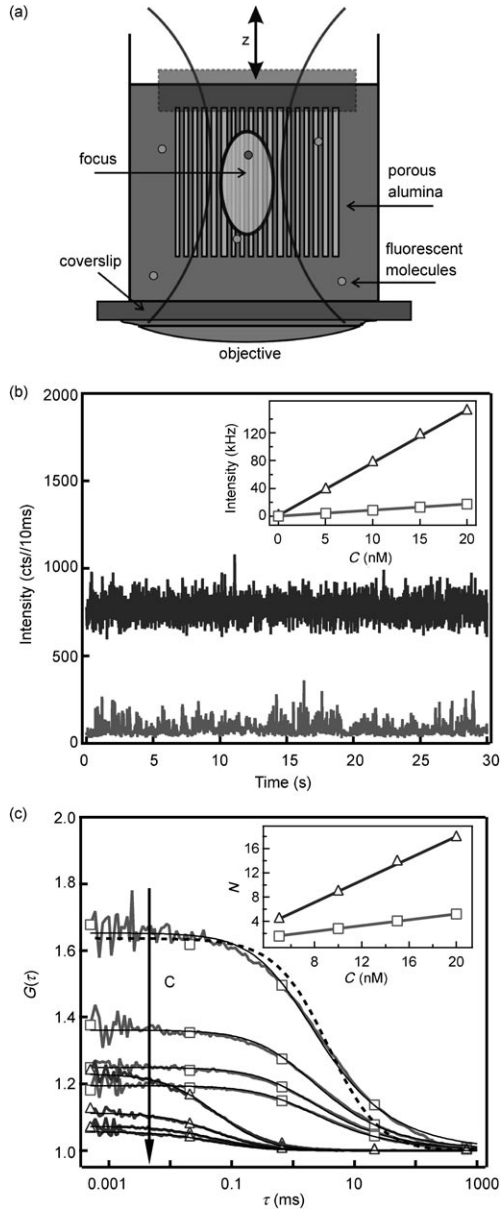

Figure 1. a) Schematic cross-sectional view of the sample geometry (not to scale). The membrane was glued to a glass tube, which was attached to a linear actuator (M-230.10, PI, Karlsruhe, Germany) to adjust the spacing between the membrane and the coverslip to about 100 μm. For measurements inside the membrane the focus of the objective was moved 10 μm inside the membrane (view from the coverslip); for measurements in solution the focus was placed 20 μm below the water/membrane interface. b) Transient confocal fluorescence intensities for the dye Alexa Fluor 488 10 nM in bulk solution (top trace) and nanopore-confined solution (bottom trace) excited at 470 nm with a power of 8 μW. The inset shows the average intensity for different dye concentrations in bulk solution (triangles) and inside the nanopores (squares). Straight lines are linear fits. c) Intensity autocorrelation functions for transients of different dye concentrations in bulk solution (triangles) and in the nanopores (squares). The arrow indicates increasing concentration. The solid lines are fits according to Equation (3) assuming 3D and 1D diffusion, respectively. The dotted line exemplarily shows a fit of a 3D model to the ACF for pore-confined solution. Mean molecule numbers N in the confocal volume as a function of dye concentration are plotted in the inset in bulk solution (triangles) and inside the nanopores (squares).

(GFP, 27 kDa), which has an increased fluorescence intensity in comparison to wild-type GFP. GFP forms a barrel-like structure of about 2 nm in diameter and 4 nm in height surrounding the *p*-hydroxybenzylidene imidazolinone fluorophore.[22,23] Alexa Fluor 488 is a rhodamine-like dye, which is known to have a high quantum yield, high photostability, and a very low intersystem-crossing quantum yield.[24] The corresponding diffusion coefficients in aqueous solution are $D_{\mathrm{Alexa}} = 2.8 \times 10^{-6}\ \mathrm{cm^2\,s^{-1}}$ (measured against the chemically similar dye rhodamine 6G as a reference[25]) and $D_{\mathrm{EGFP}} = 8.7 \times 10^{-7}\ \mathrm{cm^2\,s^{-1}}$.[25]

Figure 1b shows the transient fluorescence intensity for a 10 nM solution of Alexa Fluor 488 in buffer inside the membrane, and, for comparison, in bulk solution. Both transients can be recorded for one and the same stock because our experimental setup allows for locating the detection volume inside and below the alumina membrane, respectively (see sketch in Figure 1a). Before recording the transient intensities, equilibration was evidenced by a constant time-averaged fluorescence intensity.

The two transients clearly differ in the average intensity: 77 kHz in bulk solution and 9 kHz within the membrane. The detected intensity depends linearly on the dye concentration. The ratio between the slopes of the plots showing the fluorescence intensities inside the membrane and in the bulk as a function of the concentration is 1 to 9 (Figure 1b, inset). Similar behavior is found for EGFP, the second analyte we investigated, although with a smaller ratio between the slopes of 1 to 4 (Figure 2a, inset).

The intensity drop inside the membrane could be caused by either one or a combination of the following effects: a lower average number of molecules in the detection volume, a reduced excitation intensity, a quenched emissive rate of the molecules, or a reduced detection efficiency. The first effect concerns just the apparent concentration whereas the latter three would change the molecular brightness, that is, the apparent fluorescence intensity per molecule. We will elaborate on the actual effects in detail in the following.

First, we will focus on the apparent sample concentration. In fluorescence correlation spectroscopy (FCS),[8] the fluctuating intensity (Figure 1b) is analyzed in terms of the intensity autocorrelation function (ACF)

$$G(\tau) = 1 + \frac{\langle \delta I(t) \cdot \delta I(t+\tau) \rangle}{\langle I \rangle} \tag{1}$$

where $\delta I(t)$ is the difference between the fluctuating intensity $I(t)$ and the time-averaged intensity $\langle I \rangle$. Assuming a three-dimensional (3D) Gaussian for the instrument point spread function with half axes w_0 and z_0,[26]

$$I = I_0 \exp\left(-2\left(\frac{x^2+y^2}{w_0^2} + \frac{z^2}{z_0^2}\right)\right) \tag{2}$$

and further assuming time-stationarity, the autocorrelation function reads

$$G_{3D}(\tau) = 1 + \frac{1}{N}\left(1 + \frac{4D\tau}{w_0^2}\right)^{-1}\left(1 + \frac{4D\tau}{z_0^2}\right)^{-1/2} \tag{3}$$

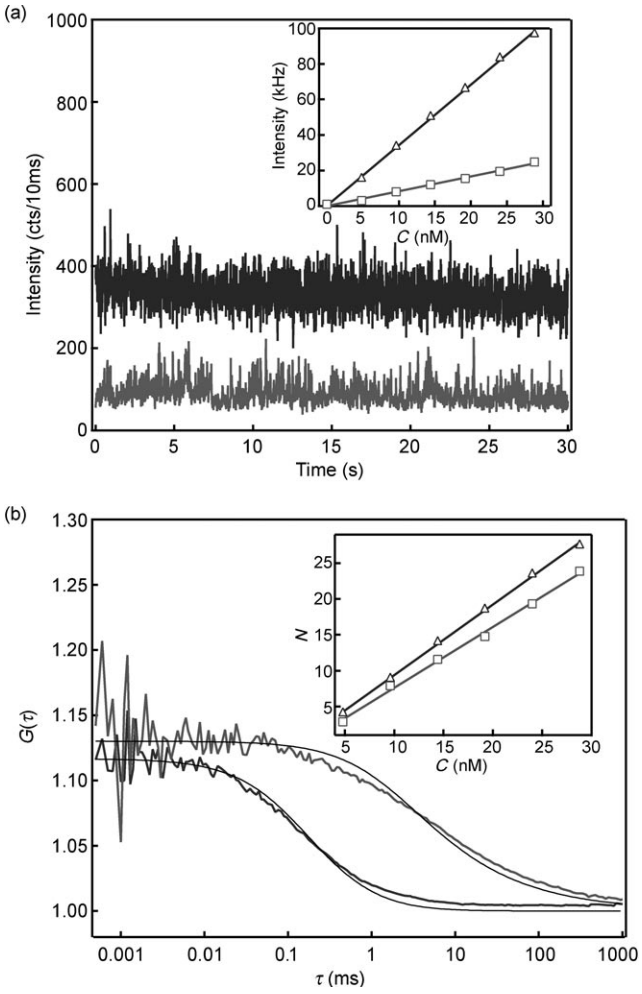

Figure 2. a) Transient confocal fluorescence intensities for the autofluorescent protein EGFP in bulk solution (top trace) and in nanopore-confined solution (bottom trace). The inset shows the average intensity for different dye concentrations in bulk solution (triangles) and inside the nanopores (squares). b) Intensity autocorrelation functions for the transient at 10 nM EGFP concentration in bulk solution (triangles) and in the nanopores (squares). The solid lines are fits according to Equation (3) assuming 3D and 1D diffusion, respectively. Mean molecule numbers N in the confocal volume as a function of protein concentration in the bulk solution (triangles) and inside the nanopores (squares) are plotted in the inset.

if the intensity fluctuations are of purely diffusive nature. Here, N represents the mean molecule number in the detection volume and D the diffusion coefficient. In our microscope, the short half-axis of the instrument point-spread function amounts to $w_0 \approx 250$ nm and the long half axis to $z_0 \approx 1000$ nm as determined by confocal imaging of fluorescent spheres embedded in agarose gel. We should emphasize that the point-spread function in the alumina membrane is identical to that in water if the spherical aberrations are corrected for using the coverglass correction ring as mentioned above.

The quantity related to the apparent concentration is the amplitude $1/N$ of the ACFs (Figure 1c), which increases with decreasing dye concentration and is considerably lower in the bulk solution than within the membrane. The obtained average number of dye molecules in the detection volume N is plotted versus the dye concentration in the inset of Figure 1c. A linear dependence is obtained, where the slope for the bulk data is about three times the slope within the membrane. Therefore, the apparent molecule number in the membrane is lower by a factor of three. This result is in reasonable agreement with the reduced detection volume inside the membrane with a porosity of 20–25%.

In contrast, we find for EGFP an apparent molecule number in the focus that essentially matches that in bulk solution (Figure 2b). Considering the transient intensity in Figure 2a, an increased background signal as compared to Alexa Fluor 488 is prominent. It is known that the uncorrelated background, which we assign to immobilized EGFP molecules, has a huge impact on the apparent mean number of molecules.[27] The assignment of the background signal to immobilized molecules is strengthened by the finding that for EGFP the average count rate is not reduced as much as for the Alexa dye. The integral intensity from membranes soaked with EGFP solution is thus the sum of diffusing molecules (as measured by FCS) and of immobilized molecules. Assuming a reduction of the effective confocal volume as for the Alexa dye, we can estimate the number of molecules causing the constant background. We find that the number of immobilized molecules in the confocal volume equals that of the mobile fraction (see Supporting Information). On the other hand, assuming a tenth of a monolayer of BSA[21] at the pore walls one can estimate that some ten thousand BSA molecules are located within the detection volume based on geometry considerations. The fraction of immobilized EGFP molecules related to the total amount of adsorbed protein is thus extremely small. Here, we additionally assume that the emitted fluorescence intensity is the same for diffusing and immobilized molecules, respectively, that is, no fluorescence quenching occurs.

We can now calculate the ratio of molecular brightness of membrane-confined and freely diffusing molecules, respectively. For the Alexa dye, the molecular brightness is reduced by a factor of 2.3, and for EGFP by a factor of 3.4 (see Supporting Information). The molecular brightness is influenced by changes in excitation intensity and detection efficiency, respectively, and by quenching of fluorescence.

In order to elucidate quenching effects due to pore–wall interactions, we studied the fluorescence decay time of the dyes in the membrane and compared it to the decay time in bulk solution. Contact with the pore walls may lead to fluorescence quenching, which can be experimentally identified by a shortening of the fluorescence decay time. Besides quenching processes the refractive index of the medium surrounding the emitter can modify the fluorescence lifetime τ_f via the radiative lifetime $\tau_0 = 1/k_{rad}$, which is indirectly proportional to the square of the refractive index.[28]

For Alexa Fluor 488 the fluorescence decays follow a single-exponential law showing up as straight lines in the semilogarithmic plot in Figure 3a. We find a decrease of the fluorescence lifetime from $\tau_{f,H_2O} = 4.1$ ns in bulk solution to $\tau_{f,M} = 3.0$ ns within the membrane for all dye concentrations.

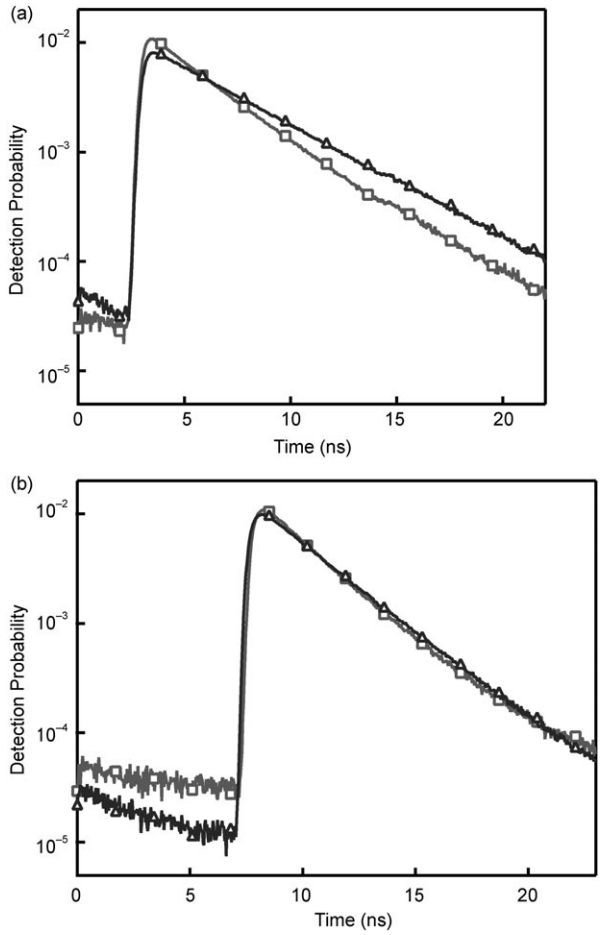

Figure 3. a) Fluorescence decay for 10 nM Alexa Fluor 488 in bulk solution (triangles) and in the nanoporous membrane (squares). b) Fluorescence decay for 10 nM EGFP in bulk solution (triangles) and in the nanoporous membrane (squares).

For Alexa Fluor 488 with its fluorescence quantum yield close to unity in solution, the fluorescence decay is almost exclusively governed by the radiative rate. With the refractive index of $n=1.57$ for the water-filled membrane we expect a fluorescence lifetime of $\tau_{f;M}=2.9$ ns, which almost perfectly matches the experimental result. We thus reason that the pore–wall modification with BSA prevents collisional quenching processes.

For EGFP (Figure 3b), we apply a monoexponential-fit model, which reflects the shortening of the fluorescence decay due to refractive-index changes following Suhling's approach.[29] We obtain a fluorescence lifetime of $\tau_{f,H_2O}=2.6$ ns in the bulk solution and $\tau_{f;M}=2.2$ ns in the membrane. The quantum yield of fluorescence $\Phi_f=k_{rad}/(k_{rad}+k_{nrad})=k_{rad}\tau_f$ for EGFP is $\Phi_f=0.6$.[30] Combining the Strickler–Berg formula with the definition of the fluorescence quantum yield,

$$\tau_{f,M}=\left(\frac{\Phi_f}{\tau_{f,H_2O}}+\frac{1-\Phi_f}{\tau_{f,H_2O}}\frac{n_M^2}{n_{H_2O}^2}\right)^{-1} \quad (4)$$

we estimate a fluorescence decay time in the membrane of $\tau_{f;M}=2.2$ ns, which is again in perfect agreement with the experimental results and indicative of the absence of quenching processes. At first, this finding is surprising because there are immobilized molecules in the membrane that might be prone to quenching. The chromophore of EGFP, however, appears to be shielded by the protein structure from the environment, thus preventing collisional quenching by pore–wall contacts.

Having ruled out fluorescence quenching as the reason for the reduction of the molecular brightness in the membrane, only effects of excitation and detection remain. The excitation intensity is not significantly altered in the membrane due to the coverglass correction of the microscope objective. However, the aperture angle for detection is only 50° in the membrane as compared to 64° in water. This leads to a reduction in collection efficiency by a factor of ≈1.6. The slightly higher reduction of molecular brightness observed is probably caused by remaining optical aberrations because of the difference of the refractive indices of glass and water-filled nanoporous alumina.

We now concentrate on the dwell time of the molecules in the focal volume, which is related to the decay of the ACFs shown for Alexa Fluor 488 solutions in Figure 1c. If we assume 1D diffusion along the z axis due to the channel confinement, the first term in parentheses in Equation (3) vanishes. The solid lines in Figure 1c represent fits to the experimental ACFs with the 1D model for the signal measured inside the membrane and with the 3D model in bulk solution, respectively. All ACFs have been corrected for after-pulsing by application of a temporal filter.[31] The excellent agreement of the fitted curves and the experimental autocorrelation functions for the transients taken inside the nanopores is evidence of apparent 1D diffusion. No long-time component is obvious in the ACFs, demonstrating the absence of sticking effects. Defining the diffusion time for the unconfined diffusion as $\tau_D^{3D}=w_0^2/4D$ and for 1D diffusion as $\tau_D^{1D}=z_0^2/4D$, the ratio between the diffusion time in the 1D case along z and in the 3D case is simply the square of the structural parameter s, which is defined as $s=z_0/w_0$ and amounts to $s\approx4$ in the microscope used. Assuming the same diffusion coefficient in bulk and pore water, respectively, we therefore expect a τ_D inside the membrane that is 16 times longer compared to free bulk diffusion. The ratio between the visually easier-to-access ACF decay half times $\tau_{1/2}$, however, is even larger due to the different exponents of the diffusion terms.

The fits of the model functions (Eq. (3)) to the experimental ACFs yield diffusion times τ_D of $\tau_D^{3D}=(54\pm3)$ μs in bulk solution and $\tau_D^{1D}=(1003\pm30)$ μs in the membrane with negligible variations between the different concentrations. The diffusion time τ_D in the membrane is thus 19 times longer than in free solution. This is in reasonable agreement with the model we apply and moreover indicates that the diffusion time of Alexa Fluor 488 molecules is not affected by interactions between the analyte and the pore walls and that its diffusion coefficient is not altered due to confinement. The same holds for EGFP, where we find a 14-fold increased diffusion time in the membrane as compared to the bulk solution. We can only speculate that the deviations of the experimental ACFs from the model functions in solution

as well as under confinement for EGFP (Figure 2b) are related to the inherent photophysics of the EGFP chromophore.[32]

In summary, we have demonstrated that functionalized nanoporous alumina can be applied for single-molecule fluorescence detection in nanoscale confinement. The confinement leads to apparent 1D diffusion with up to 19-fold prolonged diffusion times through the focus. The sensitivity of sticking to the pore walls depends on the chemical composition of the molecules under study. Changes in the diffusion coefficient in even smaller pores may also be detected by this technique. Single-molecule fluorescence in porous alumina is a promising tool for the study of dynamical processes in macromolecular systems and for highly parallel ultrasensitive analytical applications. The robustness and relative ease-of-use of our approach will be advantageous in this respect. Moreover, the technique allows for the evaluation of functionalized nanoporous devices for sensing and filtration with unsurpassed detail.

Experimental Section

A confocal optical microscope (Zeiss Confocor 1, objective 40× magnification, NA 1.2 water, C-Apochromat) was used for the experiments and was upgraded with a pulsed diode laser emitting at 470 nm (PDL 470, PicoQuant, Berlin, Germany). The driving circuitry (PDL800-B PicoQuant, Berlin, Germany) provided electrical pulses synchronously with light pulses necessary to perform time-correlated single-photon counting (TCSPC). The repetition rate of the laser was set to 40 MHz. A single-photon avalanche photodiode (SPCM AQ-14, Perkin–Elmer, MA, US) was used as the detector. The pulses from the detector and the synchronous pulses from the laser driver were fed into a TCSPC board (TimeHarp 200, PicoQuant, Berlin, Germany) operated in the time-tagged, time-resolved mode, providing a timing resolution of 39 ps for recording the fluorescence decay and 100-ns resolution for recording photon arrival times. The overall instrument-response function had a full width at half-maximum of 550 ps. Laser light was linearly polarized with an intensity of about 8 μW. For further descriptions of the confocal optical microscope see Reference [19].

Highly ordered porous alumina was prepared following the procedures described elsewhere.[1,33] The second anodization in 0.3 M sulfuric acid solution took 7 h, yielding pores with a diameter of 25 nm and a depth of ≈35 μm. The pores were then widened to 35–40 nm, as determined by scanning electron microscopy (data not shown), by isotropic etching with 0.3 M oxalic acid for 1 h at 30 °C. We temporarily protected the surface of the membrane with a polymeric coating and removed the underlying aluminum substrate connected with the alumina membrane by a selective wet-chemical etching step with a mixture of 1.7 g $CuCl_2$–H_20, 50 mL concentrated HCl, and 50 mL deionized water. Then, the remaining membrane was treated with 10% phosphoric acid at 30 °C for some minutes. By this isotropic etching step the barrier oxide at the pore bottoms was removed so that the pores were open at both ends. The membrane was glued to a glass tube, which was attached to a linear actuator (M-230.10, PI, Karlsruhe, Germany) to adjust the spacing between the membrane and the coverslip to about 100 μm. For measurements inside the membrane the focus of the objective was moved 10 μm inside the membrane (view from the coverslip); for measurements in solution the focus was placed 20 μm below the water/membrane interface. Before any measurement the membranes and the chamber were incubated with 107 μM bovine serum albumine in order to prevent unspecific adsorption on the fluorescent molecules. After incubation the membranes were rinsed with deionized water. For use in the experiments the dye Alexa Fluor 488 (Invitrogen, Carlsbad, CA, US) and EGFP were dissolved in 10 mM phosphate buffered saline (PBS) buffer (+137 mM NaCl, +2.7 mM KCl, pH 7.4, Sigma–Aldrich). EGFP was expressed as a $(His)_{10}$ fusion using the pET19b-EGFP expression plasmid in *E. coli* BL21 (DE3) cells at 25 °C and purified as described.[34]

Keywords:
diffusion · membranes · nanopores · ordered structures · single-molecule studies

[1] H. Masuda, K. Fukada, *Science* **1995**, *268*, 1466–1468.
[2] K. Nielsch, J. Choi, K. Schwirn, R. B. Wehrspohn, U. Gösele, *Nano Lett.* **2002**, *2*, 677–681.
[3] A. Yamaguchi, F. Uejo, T. Yoda, T. Uchida, Y. Tanamura, T. Yamashita, N. Teramae, *Nat. Mater.* **2004**, *3*, 337–341.
[4] H. Yang, A. Kuperman, N. Coombs, S. Mamiche Afara, G. Ozin, *Nature* **1996**, *379*, 703–705.
[5] Y. Fu, F. Ye, W. G. Sanders, M. M. Collinson, D. A. Higgins, *J. Phys. Chem. B* **2006**, *110*, 9164–9170.
[6] S. M. Mahurin, S. Dai, M. D. Barnes, *J. Phys. Chem. B* **2003**, *107*, 13336–13340.
[7] C. Seebacher, C. Hellriegel, F. W. Deeg, C. Bräuchle, S. Altmaier, P. Behrens, K. Müllen, *J. Phys. Chem. B* **2002**, *106*, 5591–5595.
[8] D. Magde, E. Elson, W. W. Webb, *Phys. Rev. Lett.* **1972**, *29*, 705–709.
[9] J. K. Holt, H. G. Park, Y. Wang, M. Stadermann, A. B. Artyukhin, C. P. Grigoropoulos, A. Noy, O. Bakajin, *Science* **2006**, *312*, 1034–1037.
[10] A. M. Kelley, X. Michalet, S. Weiss, *Science* **2001**, *292*, 1671–1672.
[11] B. Schuler, E. A. Lipman, W. A. Eaton, *Nature* **2002**, *419*, 743–747.
[12] A. A. Deniz, T. A. Laurence, G. S. Beligere, M. Dahan, A. B. Martin, D. S. Chemla, P. E. Dawson, P. G. Schultz, S. Weiss, *Proc. Natl. Acad. Sci. USA* **2000**, *97*, 5179–5184.
[13] E. A. Lipman, B. Schuler, O. Bakajin, W. A. Eaton, *Science* **2003**, *301*, 1233–1235.
[14] N. Baudendistel, G. Müller, W. Waldeck, P. Angel, J. Langowski, *ChemPhysChem* **2005**, *6*, 984–990.
[15] P. Schwille, F. J. Meyer-Almes, R. Rigler, *Biophys. J.* **1997**, *72*, 1878–1886.
[16] M. J. Levene, J. Korlach, S. W. Turner, M. Foquet, H. G. Craighead, W. W. Webb, *Science* **2003**, *299*, 682–686.
[17] M. Foquet, J. Korlach, W. R. Zipfel, W. W. Webb, H. G. Craighead, *Anal. Chem.* **2004**, *76*, 1618–1626.
[18] H. Masuda, F. Hasegawa, S. Ono, *J. Electrochem. Soc.* **1997**, *144*, L127–L130.
[19] A. Benda, M. Hof, M. Wahl, M. Patting, R. Erdmann, P. Kapusta, *Rev. Sci. Instrum.* **2005**, *76*, 033106.
[20] J. Hohlbein, U. Rehn, R. B. Wehrspohn, *Phys. Status Solidi A* **2004**, *201*, 803–808.

[21] K. H. A. Lau, L. S. Tan, K. Tamada, M. S. Sander, W. Knoll, *J. Phys. Chem. B* **2004**, *108*, 10812 – 10818.
[22] B. P. Cormack, R. H. Valdivia, S. Falkow, *Gene* **1996**, *173*, 33 – 38.
[23] M. Ormö, A. B. Cubitt, K. Kallio, L. A. Gross, R. Y. Tsien, S. J. Remington, *Science* **1996**, *273*, 1392 – 1395.
[24] N. Panchuk-Voloshina, R. P. Haugland, J. Bishop-Stewart, M. K. Bhalgat, P. J. Millard, F. Mao, W. Y. Leung, R. P. Haugland, *J. Histochem. Cytochem.* **1999**, *47*, 1179 – 1188.
[25] B. R. Terry, E. K. Matthews, J. Haseloff, *Biochem. Biophys. Res. Commun.* **1995**, *217*, 21 – 27.
[26] R. Rigler, U. Mets, J. Widengren, P. Kask, *Eur. Biophys. J.* **1993**, *22*, 169 – 175.
[27] D. E. Koppel, *Phys. Rev. A* **1974**, *10*, 1938 – 1946.
[28] S. J. Strickler, R. A. Berg, *J. Chem. Phys.* **1962**, *37*, 814 – 822.
[29] K. Suhling, J. Siegel, D. Phillips, P. M. W. French, S. Leveque-Fort, S. E. D. Webb, D. M. Davis, *Biophys. J.* **2002**, *83*, 3589 – 3595.
[30] G. H. Patterson, S. M. Knobel, W. D. Sharif, S. R. Kain, D. W. Piston, *Biophys. J.* **1997**, *73*, 2782 – 2790.
[31] J. Enderlein, I. Gregor, *Rev. Sci. Instrum.* **2005**, *76*, 033102.
[32] U. Haupts, S. Maiti, P. Schwille, W. W. Webb, *Proc. Natl. Acad. Sci. USA* **1998**, *95*, 13573 – 13578.
[33] A. Li, F. Müller, A. Birner, K. Nielsch, U. Gösele, *J. Appl. Phys.* **1998**, *84*, 6023 – 6026.
[34] A. Malik, R. Rudolph, B. Söhling, *Anal. Biochem.* **2005**, *340*, 252 – 258.

Received: August 4, 2006
Revised: October 17, 2006
Published online on February 7, 2007

